JACS
JOURNAL OF THE AMERICAN CHEMICAL SOCIETY
pubs.acs.org/JACS
Article

Divalent Lanthanide Metallocene Complexes with a Linear Coordination Geometry and Pronounced 6s−5d Orbital Mixing

K. Randall McClain,○ Colin A. Gould,○ David A. Marchiori, Hyunchul Kwon, Trisha T. Nguyen, Kyle E. Rosenkoetter, Diana Kuzmina, Floriana Tuna, R. David Britt, Jeffrey R. Long,* and Benjamin G. Harvey*

Cite This: *J. Am. Chem. Soc.* 2022, 144, 22193−22201

Read Online

ACCESS | Metrics & More | Article Recommendations | Supporting Information

ABSTRACT: A small but growing number of molecular compounds have been isolated featuring divalent lanthanides with $4f^n5d_{z^2}^1$ electron configurations. While the majority of these possess trigonal coordination geometries, we previously reported the first examples of linear divalent metallocenes $Ln(Cp^{iPr5})_2$ (Ln = Tb, Dy; Cp^{iPr5} = pentaisopropylcyclopentadienyl). Here, we report the synthesis and characterization of the remainder of the $Ln(Cp^{iPr5})_2$ (**1-Ln**) series (including Y and excluding Pm). The compounds can be synthesized through salt metathesis of LnI_3 and $NaCp^{iPr5}$ followed by potassium graphite reduction for Ln = Y, La, Ce, Pr, Nd, Gd, Ho, and Er, by *in situ* reduction during salt metathesis of LnI_3 and $NaCp^{iPr5}$ for Ln = Tm and Lu, or through salt metathesis from LnI_2 and $NaCp^{iPr5}$ for Ln = Sm, Eu, and Yb. Single crystal X-ray diffraction analyses of **1-Ln** confirm a linear coordination geometry with pseudo-D_{5d} symmetry for the entire series. Structural and ultraviolet−visible spectroscopy data support a $4f^{n+1}$ electron configuration for Ln^{2+} = Sm, Eu, Tm, and Yb and a $4f^n5d_{z^2}^1$ configuration for the other lanthanides ($[Kr]4d_{z^2}^1$ for Y^{2+}). Characterization of **1-Ln** (Ln = Y, La) using electron paramagnetic resonance spectroscopy reveals significant s−d orbital mixing in the highest occupied molecular orbital and hyperfine coupling constants that are the largest reported to date for divalent compounds of yttrium and lanthanum. Evaluation of the room temperature magnetic susceptibilities of **1-Ln** and comparison with values previously reported for trigonal Ln^{2+} compounds suggests that the more pronounced 6s−5d mixing may be associated with weaker 4f−5d spin coupling.

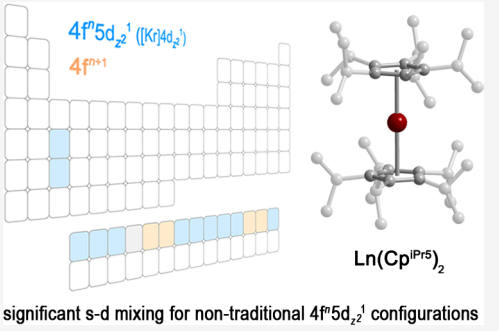

INTRODUCTION

The chemistry of the lanthanide elements and yttrium is generally dominated by the trivalent oxidation state.[1] Indeed, prior to the mid-1990s, molecules containing divalent lanthanide ions had only been reported for Sm, Eu, and Yb. For these elements, reduction leads to stable electron configurations wherein the 4f orbitals are nearly half-filled (Sm), half-filled (Eu), or fully filled (Yb),[2] and as such they possess the highest Ln^{3+}/Ln^{2+} reduction potentials of the lanthanide series. The dearth of compounds featuring the other divalent lanthanides led to speculation that such species could not be isolated;[2] however, efforts in recent years have overturned this assumption, and complexes containing divalent metal ions have been realized for the entire lanthanide series and yttrium, which is commonly grouped with the rare earths.[3−9] This work has significantly expanded our understanding of these elements, revealing unforeseen chemical reactivity[10] and enabling access to unique electronic[11] and magnetic properties.[12]

One intriguing aspect of divalent lanthanides in molecular compounds is their electronic structure. While so-called classical divalent lanthanide ions Sm^{2+}, Eu^{2+}, and Yb^{2+} (and typically Tm^{2+}) possess a $4f^{n+1}$ electron configuration, the remainder of the lanthanides (and yttrium) can sometimes possess a $4f^n5d_{z^2}^1$ ($[Kr]4d_{z^2}^1$) configuration wherein the added electron resides in a d_{z^2} orbital.[5−9] Electron configurations in which unpaired electrons populate two different, partially filled valence shells on the same atom are rare for molecular complexes and constitute an exception to the Aufbau principle, and the $4f^n5d_{z^2}^1$ configuration in divalent lanthanide complexes gives rise to unusual properties. For instance, $[K(2,2,2\text{-cryptand})][LnCp'_3]$ (Ln = Dy, Ho; Cp′ = $C_5H_4SiMe_3$)[13] exhibit record-high single-ion magnetic moments and the neutral metallocenes $Ln(Cp^{iPr5})_2$ (Ln = Dy, Tb; Cp^{iPr5} = pentaisopropylcyclopentadienyl) exhibit high-symmetry linear coordination geometries as a result of $4f^n5d_{z^2}^1$ configurations.[14] In the case of $Tb(Cp^{iPr5})_2$, the molecular symmetry in tandem with the Kramers ground state of the highly anisotropic Tb^{2+} ion gives rise to the second highest magnetic blocking

Received: September 15, 2022
Published: November 23, 2022

https://doi.org/10.1021/jacs.2c09880
J. Am. Chem. Soc. 2022, 144, 22193−22201

temperature to date for a single-molecule magnet not based on dysprosium.[14] In addition, salts of the molecular qubit candidates $[MCp'_3]^-$ (M = Y, La, Lu) display long coherence times as a result of $4f^n5d_{z^2}^1$ ($[Kr]4d_{z^2}^1$ for yttrium) electron configurations and significant 6s−5d (5s−4d) mixing, which minimizes spin anisotropy.[11] Recently, we also discovered that the mixed-valence dilanthanide compounds $(Cp^{iPr5})_2Ln_2I_3$ (Ln = Gd, Tb, Dy) exhibit Robin−Day Class III mixed valence arising from the presence of a singly occupied σ-bonding orbital of Ln $5d_{z^2}$ parentage, which imparts strong parallel alignment of the 4f and 5d electrons and record coercive magnetic fields for Tb and Dy.[12] Further studies of divalent lanthanide complexes are essential toward understanding and optimizing their electronic and magnetic properties.

Herein, we report the synthesis and characterization of the neutral metallocenes $Ln(Cp^{iPr5})_2$ (**1-Ln**) for the entire lanthanide series (La−Lu, including Y and excluding Pm), building upon our previous communication of the synthesis, magnetism, and preliminary analysis of the electronic structure of $Tb(Cp^{iPr5})_2$ and $Dy(Cp^{iPr5})_2$.[14] While the vast majority of reported divalent lanthanide complexes possess a trigonal coordination environment, **1-Ln** possess a linear, pseudo-D_{5d} geometry and are the first examples of neutral linear metallocenes for ten new elements, Y, La, Ce, Pr, Nd, Gd, Ho, Er, Tm, and Lu. Characterization of these compounds via single-crystal X-ray diffraction analysis, cyclic voltammetry, UV−vis and EPR spectroscopies, and magnetic susceptibility measurements reveals trends in electronic structure, including insights into the valence orbital occupancies that impact internal spin−spin coupling.

RESULTS AND DISCUSSION

Synthesis and Structural Characterization. We previously reported the neutral, linear metallocenes $Ln(Cp^{iPr5})_2$ (Ln = Dy, Tb), which were synthesized via potassium graphite (KC_8) reduction of the putative complexes $Ln(Cp^{iPr5})_2I$, prepared from the reaction of LnI_3 and $NaCp^{iPr5}$ in toluene at high temperature.[14] This approach was inspired by reports of the reduction of Tm- or $Dy(Cp^{ttt})_2I$ (Cp^{ttt} = 1,2,4-tri(*tert*-butyl)cyclopentadienyl) with KC_8 to yield the bent metallocene $(Cp^{ttt})_2Tm(THF)$ or the iodide bridged "ate" complex $(Cp^{ttt})_2Dy(\mu\text{-}I)K(18\text{-crown-}6)$, respectively.[15,16] Gratifyingly, we were able to extend this approach to synthesize the neutral, linear metallocenes **1-Ln** for Ln = Y, La, Ce, Pr, Nd, Gd, Ho, and Er (see Scheme 1, upper, and the Supporting Information for details). In brief, the reaction of LnI_3 with 2.5 equiv of $NaCp^{iPr5}$ in toluene at high temperature for several days followed by reduction with KC_8 in benzene at room temperature yields **1-Ln**. The resulting products were crystallized from *n*-hexane to yield analytically pure red-orange (**1-Y**), dark red (**1-La**), dark green (**1-Ce**), brown-orange (**1-Pr**), brown (**1-Nd**), and orange (**1-Gd**, **1-Ho**, **1-Er**) single crystals in low to moderate yields (16% to 49%).

We attempted to isolate the putative precursor compounds $Ln(Cp^{iPr5})_2I$ using conditions similar to those used in the salt metathesis step described above (see the Supporting Information for details), but this approach met with limited success. Workup and purification of the resulting solids from *n*-hexane resulted in colorless (Y, La), red (Ce), yellow (Pr), yellow-green (Nd), yellow (Gd, Tb, Dy, Ho), or light pink (Er) crystalline material containing $Ln(Cp^{iPr5})_2I$, as verified by mass spectrometry (MALDI-ToF), although only $Ln(Cp^{iPr5})_2I$ (**2-Ln**; Ln = La, Y, Er) were obtained as analytically pure compounds via this method. We were able to devise alternative routes to obtain pure crystalline material for **2-Ln** (Ln = Ce, Pr, Nd, Gd, Tb, Dy), and full details are given in the Supporting Information. In our hands, it was not possible to isolate **2-Ho** as an analytically pure compound.

Scheme 1. (Upper) Two-Step Synthesis of 1-Ln (Ln = Y, La, Ce, Pr, Nd, Gd, Tb,[14] Dy,[14] Ho, and Er) via Salt Metathesis with $NaCp^{iPr5}$ in Toluene at Elevated Temperature Followed by Reduction with KC_8 in Benzene at Room Temperature (~25 °C) over the Course of 6 d; (Middle) Formation of 1-Ln (Ln = Tm, Lu) via *in Situ* Reduction; (Lower) Salt Metathesis Reaction To Form 1-Ln (Ln = Sm, Eu, Yb) Starting from the Divalent Lanthanide Iodides

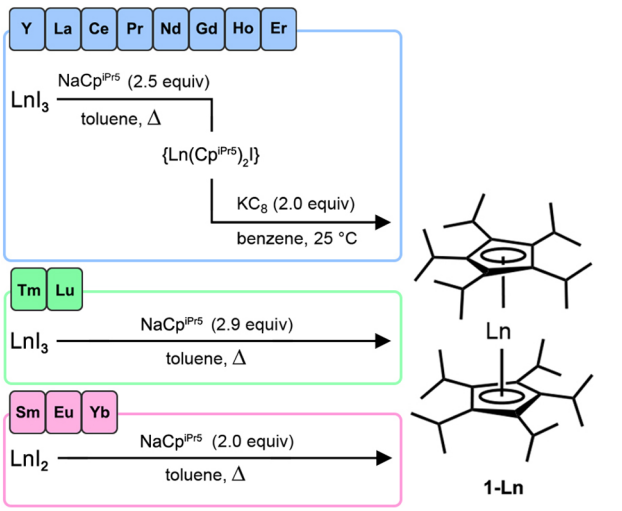

Interestingly, the salt metathesis reaction of TmI_3 with 2.5 equiv of $NaCp^{iPr5}$ under similar conditions, as used for the other lanthanides, did not yield **2-Tm**. Instead, crystallization of the resulting crude violet powder from hot benzene directly afforded violet crystals of divalent **1-Tm**. We surmise that salt metathesis between TmI_3 and $NaCp^{iPr5}$ is accompanied by *in situ* reduction of **2-Tm** by excess $NaCp^{iPr5}$ to give **1-Tm** (Scheme 1, middle). As such, the reaction was subsequently optimized by using 2.9 equiv of $NaCp^{iPr5}$ to match the expected stoichiometry more closely, affording **1-Tm** in 39% yield. Likewise, the reaction of LuI_3 with 2.9 equiv of $NaCp^{iPr5}$ in toluene at high temperature over the course of several days was found to yield **1-Lu**. Pure **1-Lu** was obtained as yellow crystals in 25% yield via crystallization from *n*-hexane.

For the remaining lanthanides in the series, Sm, Eu, and Yb, the $Ln(Cp^{iPr5})_2$ compounds have previously been reported, prepared via oxidation of the respective metal with the thermally stable pentaisopropylcyclopentadienyl radical ($\cdot Cp^{iPr5}$).[17] The resulting yields for the Sm and Yb complexes were very low; however, and only $Eu(Cp^{iPr5})_2$ was previously structurally characterized. Here, we found that **1-Sm**, **1-Eu**, and **1-Yb** could be obtained in uniformly good yield (>70%) as single crystals via stoichiometric salt metathesis reactions between LnI_2 and $NaCp^{iPr5}$ in toluene at high temperature (Scheme 1, lower). Violet (**1-Sm**), bright orange (**1-Eu**), and orange-brown (**1-Yb**) crystals were obtained from hot concentrated benzene solutions left to cool to room temperature.

All the neutral divalent metallocenes **1-Ln** display surprising thermal stability. In most cases, the purified solids were found to be stable at room temperature over many months under

https://doi.org/10.1021/jacs.2c09880
J. Am. Chem. Soc. 2022, 144, 22193−22201

argon, as either solids or hydrocarbon solutions, and the compounds can be recrystallized from boiling *n*-hexane (69 °C) without noticeable decomposition. In addition, the formation of **1-Tm** and **1-Lu** via *in situ* reduction at ≥160 °C further suggests that these two compounds are quite thermally stable.

The solid-state structures of **1-Ln** and **2-Ln** were determined from single-crystal X-ray diffraction analysis (see Figures 1 and S1−S22). Positional disorder of the Cp^{iPr5} ligand was observed for most compounds, and as a result, average Ln−C and Ln−Cp distances were calculated using the occupancy of each disordered component as a weighting factor (see Section 3 of the Supporting Information for details), yielding values that can be readily compared across the series. For **2-Ln**, the average Ln−C distance decreases monotonically from 2.853(2) Å in **2-La** to 2.660(11) Å in **2-Er** (Tables S6 and S7), as expected due to the lanthanide contraction. Similarly, the Ln−I distance decreases monotonically from 3.126(1) Å in **2-La** to 2.956(1) Å in **2-Er** (Figure 2, upper). In contrast, structural trends for **1-Ln** are not monotonic. While the average Ln−C distance in **1-Ln** decreases in a linear fashion for Ln = La, Ce, Pr, Nd, Gd, Tb, Dy, Ho, Er, and Lu, the Ln−C distances for **1-Sm**, **1-Eu**, **1-Tm**, and **1-Yb** follow a separate linear trend and are longer than those determined for adjacent members of the series (Figure 2, lower). Shorter average Ln−C and Ln−Cp distances have been reported for [K(2,2,2-cryptand)][$LnCp'_3$] compounds with a $4f^n5d_{z^2}^1$ electron configuration relative to those with a $4f^{n+1}$ configuration, as a result of covalent interactions between the populated $5d_{z^2}$ orbital and the cyclopentadienyl ligand.[7,8] Thus, these structural trends support a $4f^{n+1}$ electron configuration for **1-Sm**, **1-Eu**, **1-Tm**, and **1-Yb** and a $4f^n5d_{z^2}^1$ configuration for the remainder of the **1-Ln** series. The bond distances determined for **1-Y** are similar to those for $Dy(Cp^{iPr5})_2$,[14] as expected given the similar ionic radii of Y^{2+} and Dy^{2+}.

A comparison of the structures of **1-Ln** and **2-Ln** reveals substantial differences in the orientation of the isopropyl groups of their Cp^{iPr5} ligands. In the case of **1-Ln**, the isopropyl groups of each cyclopentadienyl ring are mutually oriented in either a slightly right- or left-facing direction to minimize steric repulsion. In contrast, the isopropyl groups in **2-Ln** are rotated out of mutual alignment to accommodate the iodide ligand and the resulting bent coordination geometry of the complex (see Figure S23). The average angle between the isopropyl groups and the plane of the cyclopentadienyl ligand is smaller in **1-Gd** than in **2-Gd** (7.6(2)° versus 9.8(2)°), and a similar trend is observed for other **1-Ln** and **2-Ln** compounds. A decrease in Cp^{iPr5} ligand strain may serve to facilitate reduction of **2-Ln** to form **1-Ln**, which may also help to explain the formation of **1-Tm** and **1-Lu** via *in situ* reduction. Indeed, based on the ionic radii of Tm^{3+} and Lu^{3+}, the putative iodide complexes $Tm(Cp^{iPr5})_2I$ and $Lu(Cp^{iPr5})_2I$ are expected to display the greatest amount of ligand strain in the series.

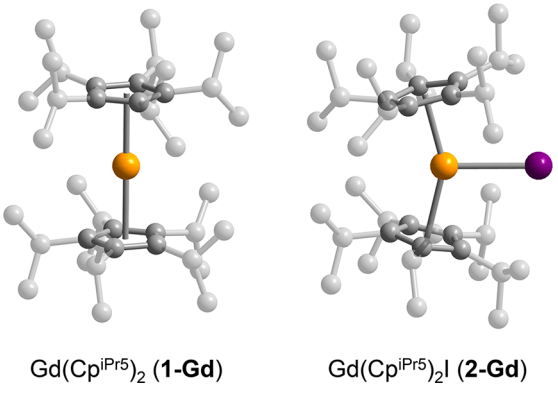

Figure 1. Single-crystal X-ray diffraction structures of **1-Gd** and **2-Gd**. Orange, gray, and purple spheres represent Gd, C, and I atoms, respectively; hydrogen atoms and positional disorder are omitted for clarity. Compounds **1-Ln** and **2-Ln** are isostructural to **1-Gd** and **2-Gd**, respectively.

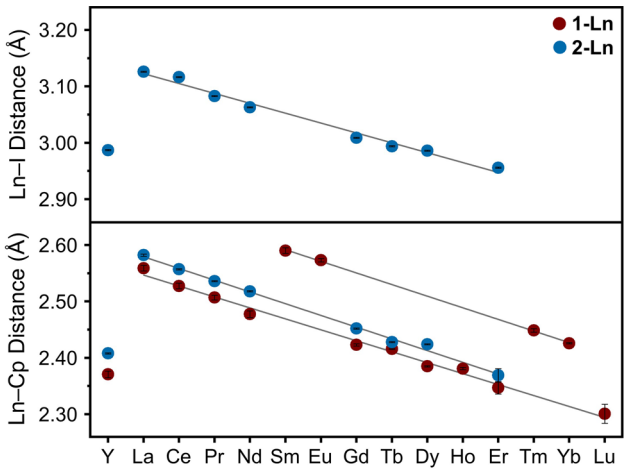

Figure 2. (Upper) Average Ln−I bond distances in **2-Ln** (blue) and (lower) average Ln−Cp bond distances (Å) in **1-Ln** (red) and **2-Ln** (blue) determined from single crystal X-ray diffraction data. The gray lines are guides for the eye.

All of the **1-Ln** compounds possess a linear coordination geometry with the Ln atom located on an inversion center, resulting in a coplanar orientation of the Cp^{iPr5} ligands and a Cp−Ln−Cp angle of 180°. While the cyclopentadienyl rings of the Cp^{iPr5} ligands show small differences in C−C bond distances, the $LnCp_2$ core possesses approximate D_{5d} symmetry, excluding isopropyl groups, with a dihedral angle of approximately 36° (dihedral angle ranges from 35.8(3) to 36.2(3)° in **1-Gd**). Of note, a linear geometry is uncommon for lanthanide metallocene complexes.[18−27] Even in the crystal structure of $Sm(Cp^{BIG})_2$ (Cp^{BIG} = (4-*n*Bu-$C_6H_4)_5C_5$), which features parallel Cp rings, the thermal displacement parameters of the Sm^{2+} center are expanded in the plane between the cyclopentadienyl ligands, suggesting a deviation from linearity.[26,27] In contrast, the thermal displacement parameters of the Ln^{2+} in **1-Ln** are not expanded in this manner. The linear coordination geometry of the **1-Ln** complexes likely arises from the high symmetry, steric bulk, and strong ligand field of the Cp^{iPr5} ligand.

Cyclic Voltammetry. Cyclic voltammetry (CV) data were collected for 1,2-difluorobenzene solutions of **1-Sm**, **1-Eu**, **1-Tm**, and **1-Yb** at a scan rate of 100 mV/s (see Section 4 of the Supporting Information for full experimental details). The cyclic voltammograms of **1-Sm**, **1-Tm**, and **1-Yb** feature quasireversible Ln^{3+}/Ln^{2+} redox couples with $E_{1/2}$ values of −1.14, −1.57, and −0.51 V versus Fc^+/Fc^0, respectively, whereas an irreversible Ln^{3+}/Ln^{2+} reduction occurs for **1-Eu** at −0.29 V (Figures 3 and S24−S27). These reduction potentials are significantly less negative than reported for Sm, Eu, Tm, and Yb Ln^{3+}/Ln^{2+} couples in aqueous solution (−2.26, −1.06, −2.93, and −1.86 V versus Fc^+/Fc^0, respectively).[28−30] We

https://doi.org/10.1021/jacs.2c09880
J. Am. Chem. Soc. 2022, 144, 22193−22201

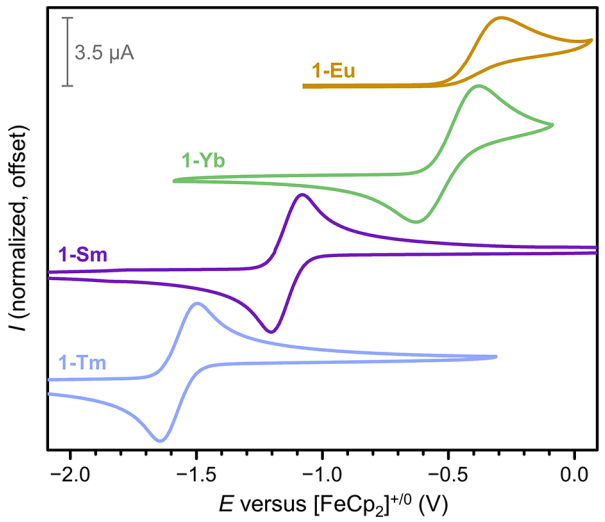

Figure 3. Cyclic voltammograms for **1-Sm** (purple), **1-Eu** (gold), **1-Tm** (blue), and **1-Yb** (green).

attribute the more accessible reductions of the **1-Ln** metallocenes to the large steric profile of the Cp^{iPr5} ligand. Relative to metallocene complexes with smaller ligands, we expect the driving force for reduction to be greater, given that reduction alleviates steric interactions by increasing the Ln−Cp^R distance and Cp^R−Ln−Cp^R angle. Reduction potentials reported for $Ln(Cp^{BIG})_2$ complexes are also lower than typically observed for other lanthanide metallocenes, supporting this hypothesis.[26] Notably, the reduction potential for **1-Tm** is less negative than the $(Cp^{iPr5})^-/(Cp^{iPr5})^\bullet$ redox couple, which occurs at −1.9 V versus Fc^+/Fc^0 in acetonitrile,[31] supporting the hypothesis that **1-Tm** is formed via reduction by $(Cp^{iPr5})^-$. Cyclic voltammetry data for the remainder of the **1-Ln** series could not be collected due to decomposition under experimental conditions; however, data were collected for $[Tb(Cp^{iPr5})_2][B(C_6F_5)_4]$,[14] which features a Tb^{3+}/Tb^{2+} redox couple with an $E_{1/2}$ value of −1.92 V versus Fc^+/Fc^0 (Figure S28).

Ultraviolet−Visible (UV−vis) Spectroscopy. UV−vis spectra were collected for hexanes solutions of **1-Ln** and **2-Ln** from 200 to 1250 nm (see Figures 4 and 5 and Section 5 of the Supporting Information). The spectra of **2-Ln** exhibit strong absorption features below 400 nm (ε > 25,000 M^{-1} cm^{-1}) that can be attributed to $\pi-\pi^*$ transitions of the cyclopentadienyl ligands. At higher wavelengths, absorption features are very weak (ε < 710 M^{-1} cm^{-1}) or absent, as expected given the Laporte-forbidden nature of f−f transitions. The spectra for **1-Sm**, **1-Eu**, **1-Tm**, and **1-Yb** also display features associated with strong $\pi-\pi^*$ transitions below 400 nm ($\varepsilon \geq$ 3200 M^{-1} cm^{-1}) and weak absorption ($\varepsilon \leq$ 1300 M^{-1} cm^{-1}) at higher wavelengths (Figure 4). These spectra are consistent with those reported previously for Ln^{2+} compounds with $4f^{n+1}$ electron configurations, which are characterized by f−d transitions in the visible region.[9,32] By contrast, the spectra for the rest of the **1-Ln** series are characterized by strong absorption ($\varepsilon \geq$ 1900 M^{-1} cm^{-1}) above 350 nm, in addition to strong $\pi-\pi^*$ absorption ($\varepsilon \geq$ 5300 M^{-1} cm^{-1}) below 350 nm (Figures 4 and 5). Such strong absorption in the visible region is consistent with UV−vis spectra reported for [K(2,2,2-cryptand)][$LnCp'_3$] compounds with $4f^n5d_{z^2}^1$ electron configurations, which display strong metal−ligand charge transfer transitions above 350 nm; however, for **1-Ln** the absorption

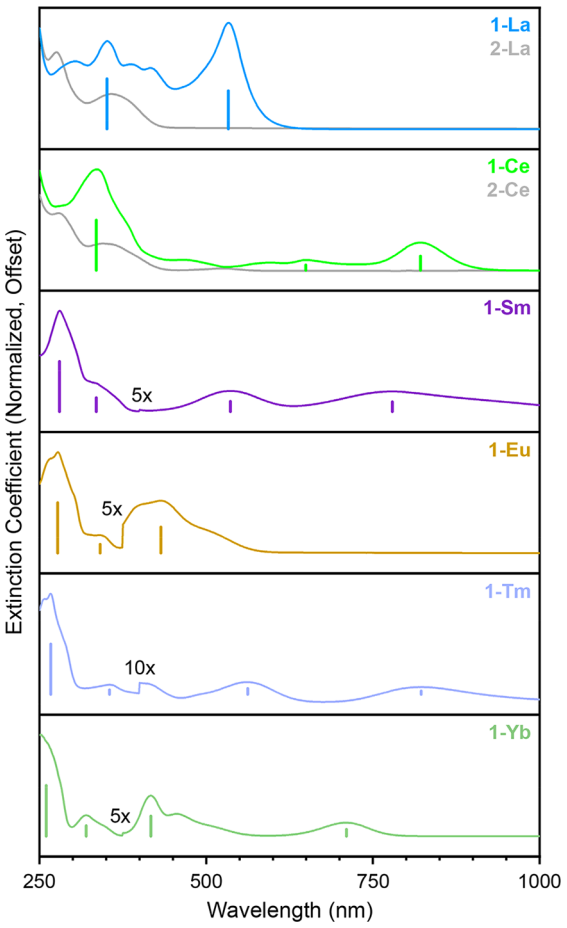

Figure 4. UV−vis spectra for **1-Ln** (Ln = La, Ce, $4f^n5d_{z^2}^1$; Sm, Eu, Tm, Yb, $4f^{n+1}$) (colored lines) and corresponding **2-Ln** compounds (gray lines). The λ_{max} value for selected absorption features for **1-Ln** are marked with vertical lines. Spectra are magnified for **1-Sm** (λ > 400 nm, 5×), **1-Eu** (λ > 375 nm, 5×), **1-Tm** (λ > 400 nm, 10×), and **1-Yb** (λ > 375 nm, 5×).

features are generally blue-shifted relative to those for [K(2,2,2-cryptand)][$LnCp'_3$].[9] The UV−vis spectra for **1-La** and **1-Ce** are unique and exhibit strong absorption features across the range of visible wavelengths (Figure 4), while the spectra for **1-Ln** (Ln = Pr, Nd, Gd, Tb, Dy, Ho, Er, Lu; Figure 5) each exhibit only one transition in the visible region with an absorption maximum that shifts to lower wavelengths (with the exception of **1-Ho** and **1-Er**) from 460 nm for **1-Pr** to 350 nm for **1-Lu**. The spectrum for **1-Lu** is noteworthy, as it is characterized by minimal absorption in the visible region, and the absorption overall is significantly blue-shifted relative to the rest of the **1-Ln** series. Finally, the UV−vis spectrum of **1-Y** (Figure 5, upper), which possesses a $[Kr]4d_{z^2}^1$ electron configuration, resembles the spectra of the other **1-Ln** (Ln = Pr, Nd, Gd, Tb, Dy, Ho, Er, and Lu). Altogether, these results support a $4f^{n+1}$ electron configuration for **1-Sm**, **1-Eu**, **1-Tm**, and **1-Yb** and a $4f^n5d_{z^2}^1$ configuration for the rest of the **1-Ln** series.

Electron Paramagnetic Resonance Spectroscopy. Continuous-wave electron paramagnetic resonance spectra were collected for frozen 3-methylpentane solutions of **1-Y**, **1-La**, and **1-Lu** at X-band frequency (9.388 GHz). The spectrum of **1-Y** obtained at 5 K features the expected doublet for an ^{89}Y nucleus ($I = {}^1/_2$), and the signal is centered at g = 1.998

https://doi.org/10.1021/jacs.2c09880
J. Am. Chem. Soc. 2022, 144, 22193−22201

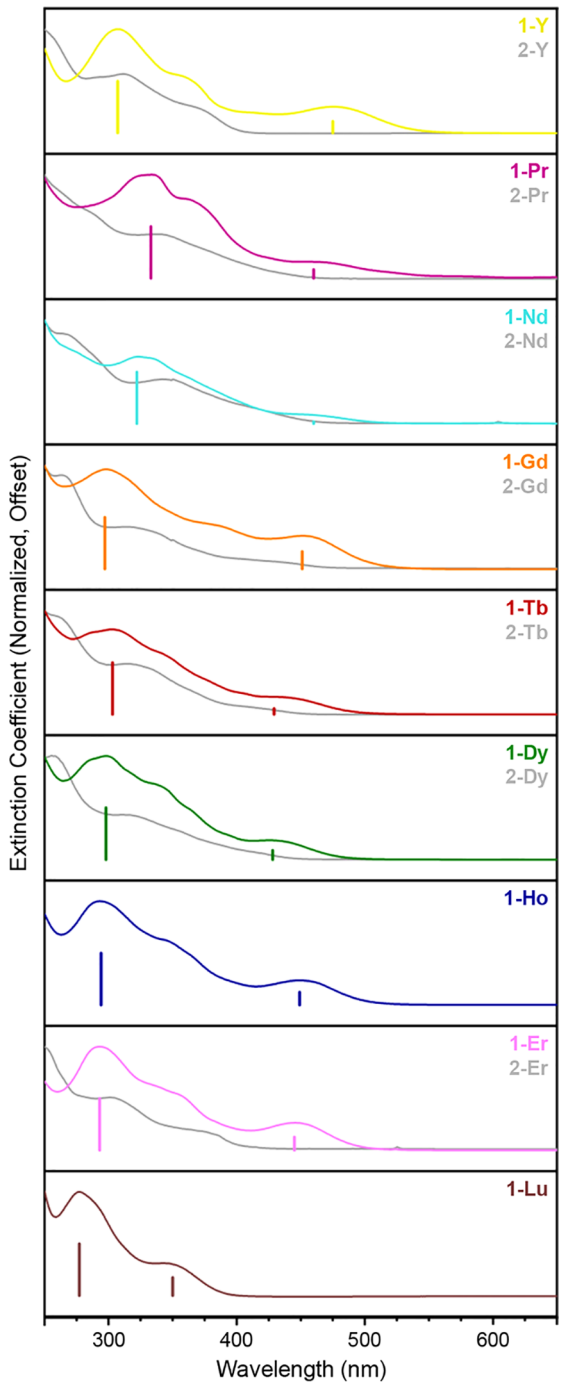

Figure 5. UV−vis spectra for **1-Ln** (Ln = Y, $4d_{z^2}^1$; Pr, Nd, Gd, Dy, Tb, Ho, Er, Lu, $4f^n5d_{z^2}^1$) and the corresponding **2-Ln** compounds (gray lines). The λ_{max} value for selected absorption features for **1-Ln** are marked with vertical lines.

(Figure 6, upper). The isotropic g factor is consistent with a $[Kr]4d_{z^2}^1$ electron configuration in which an isotropic $4d_{z^2}/5s$ orbital is the highest-occupied molecular orbital (HOMO). A fit to the data for **1-Y** yielded an isotropic hyperfine coupling constant of $a_{iso} = 5.05 \times 10^2$ MHz. Using $|A| = 1250$ MHz for the isotropic hyperfine interaction for ^{89}Y from Morton and Preston,[33] we calculated the degree of 5s−$4d_{z^2}$ mixing in the HOMO of **1-Y** ($\rho = a_{iso}/|A|$), which revealed 40.4% 5s character (see Section 6 of the Supporting Information for details). This result is consistent with prior DFT analyses of

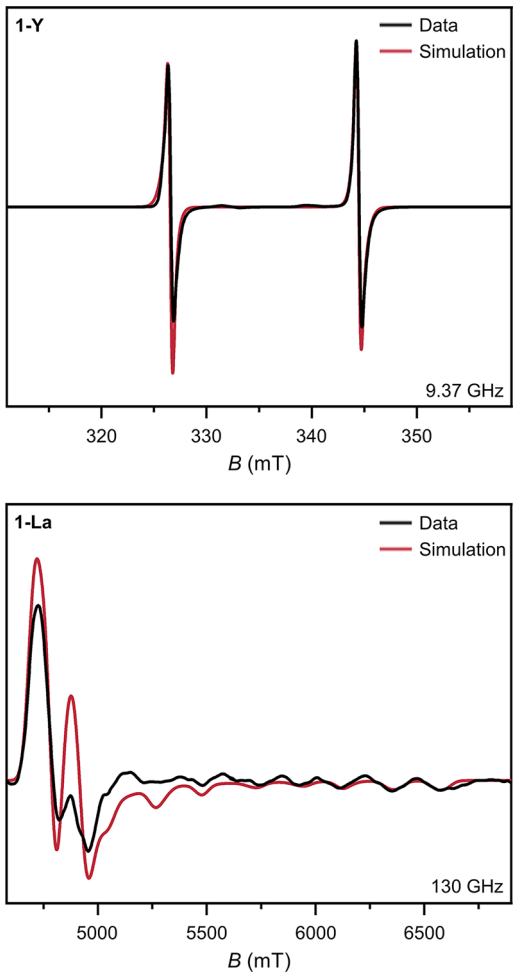

Figure 6. Experimental (black) and simulated (red) EPR spectra for **1-Y** (upper, X-band, 5 K) and **1-La** (lower, D-band, 5 K).

$Dy(Cp^{iPr5})_2$ and $Tb(Cp^{iPr5})_2$, which predicted ∼70% 6s character in the $5d_{z^2}/6s$ HOMO of these complexes.[14]

The continuous-wave X-band EPR spectra of **1-La** and **1-Lu** exhibit only weak spectral signatures (Figure S98); given the large hyperfine interaction expected for these compounds, data were also collected at D-band frequency (130 GHz) using electron spin echo methods. In the case of **1-Lu**, an electron spin echo was not observed even at 2 K, likely due to rapid spin−spin relaxation and precluding further analysis. The spectrum for **1-La** is axial with $g_\perp = 1.92$ and $g_\parallel = 1.595$, consistent with a $4f^0 5d_{z^2}^1$ electron configuration in which the HOMO is an isotropic $5d_{z^2}/6s$ orbital (Figure 6, lower). The hyperfine interaction is unresolved along $g_\perp$, but an octet is clearly visible along $g_\parallel$ (for ^{139}La, $I = {}^7/_2$). Fits to the data yielded an isotropic hyperfine coupling constant of $a_{iso} = 2.00 \times 10^3$ MHz, which corresponds to 33.3% 6s character in the HOMO (for La, $|A| = 6007$ MHz), comparable to the value determined for **1-Y**.

Altogether, EPR analysis reveals substantial s-orbital contributions to the HOMOs of **1-Y** and **1-La** that are larger than previously reported values for trigonal compounds (8.2−34.0% for Y^{2+} and 6.1−30.6% for La^{2+}; see Table S11).[6,9,34−39] Thus, changes to the ligand field and coordination geometry in nontraditional divalent lanthanide compounds can dramatically influence electronic properties. This large s-orbital mixing is what gives rise to the large isotropic hyperfine coupling

https://doi.org/10.1021/jacs.2c09880
J. Am. Chem. Soc. 2022, 144, 22193−22201

constants for **1-Y** and **1-La**, which surpass those reported to date for other compounds of Y^{2+} and La^{2+} (Table S11). We note that the approximate symmetry of **1-Ln** (D_{5d}) and $[LnCp'_3]^-$ (C_3) should restrict s−d mixing to the symmetry compatible d_{z^2} orbital. Thus, the larger s character in the HOMO of **1-Ln** is likely a consequence of a smaller energy gap between the metal-centered $5d_{z^2}$ ($4d_{z^2}$) and 6s (5s) orbitals induced by the ligand field. In support of this rationale, $[K(2.2.2\text{-crypt})][(^{Ad,Ad,t\text{-}Bu}ArO)_3Y]$ and $[K(2.2.2\text{-crypt})][Y(N(SiMe_3)_2)_3]$ exhibit greater s−d mixing and hyperfine coupling constants than [K(2,2,2-cryptand)][YCp'_3] (Table S11). However, the precise origin of the impact of ligand field and coordination geometry on s orbital character in compounds of these divalent lanthanides requires further study.

Dc Magnetic Susceptibility Measurements. Dc magnetic susceptibility data were collected for **1-Ln** (Ln = Ce, Pr, Nd, Sm, Eu, Gd, Ho, Er, Tm) from 2 to 300 K under an applied field of 10 kOe (Figure 7 and Figures S99−S106). At 300 K, the $\chi_M T$ values for **1-Eu** and **1-Tm** are 7.92 and 2.76 emu K/mol, respectively, closely matching the theoretical values for Eu^{2+} and Tm^{2+} ions with $4f^{n+1}$ electron configurations predicted based on an $L-S$ coupling scheme (7.88 or 2.57 emu K/mol, respectively, see Table 1). No measurable moment was detected for **1-Sm**, consistent with a diamagnetic ($^7F_0$) ground state predicted based on $L-S$ coupling.

In the case of the **1-Ln** compounds with $4f^n5d_{z^2}{}^1$ configurations, predicting the room temperature magnetic susceptibilities is not as straightforward. Indeed, depending on the relative strengths of the 4f and 5d spin−spin coupling and 4f spin−orbit coupling interactions, an $L-S$ coupling model may not hold. We found this to be the case based on our previous characterization of the room temperature magnetic susceptibilities of $Tb(Cp^{iPr5})_2$ and $Dy(Cp^{iPr5})_2$.[14,40] Prior analyses of the room temperature magnetic susceptibilities of the divalent lanthanide compounds [K(2,2,2-cryptand)][$LnCp'_3$] (Ln = La, Ce, Pr, Nd, Gd, Tb, Dy, Ho, Er, Lu)[13] and [K(2,2,2-cryptand)][$Ln(N(SiMe_3)_2)_3$] (Ln = Gd, Tb, Dy)[41] were carried out based on a formalism introduced by Cloke et al. to describe the magnetism of zerovalent lanthanide compounds.[42] In one of two scenarios considered (scenario 1), spin−spin coupling between the $5d_{z^2}$ and 4f electrons is assumed to be stronger than spin−orbit coupling in the 4f shell (and greater than k_BT), giving rise to an $S_{Total} = S_{4f} + {}^1/_2$ that couples with the orbital angular momentum of the 4f shell, L_{4f}, to give J_{Total}. In the second scenario (scenario 2), spin−spin coupling between the 4f and 5d electrons is assumed to be much weaker than 4f spin−orbit coupling and less than the magnitude of k_BT; in this case, the effect of the $5d_{z^2}$ electron on magnetic susceptibility was treated as an additive; that is, the predicted $\chi_M T$ value is the sum of the $\chi_M T$ value associated with the given J_{4f} and that of a free electron, 0.375 emu K/mol.

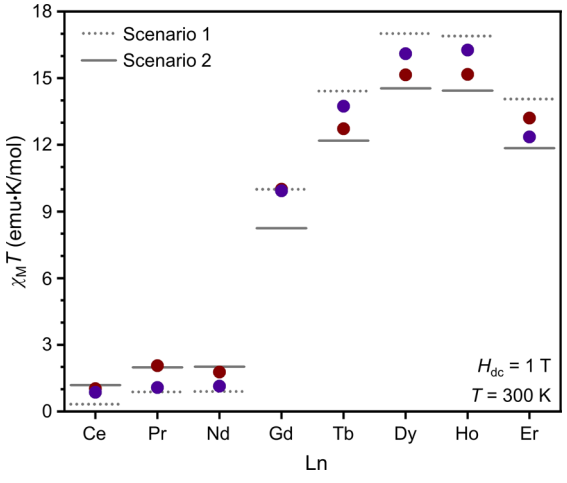

Figure 7. Experimental $\chi_M T$ values at 300 K for **1-Ln** (red circles) and previously reported trigonal divalent compounds [K(2,2,2-cryptand)][Cp'_3Ln][13] (blue circles) plotted with the predicted values based on Scenario 1 ($L-S$ coupling, dashed lines) or Scenario 2 ($J-s$ coupling, solid lines).

Table 1. Experimental (Exp.) Room Temperature $\chi_M T$ Values for 1-Ln and Predicted $\chi_M T$ Values for Three Possible Spin-Orbit Coupling Scenarios[a]

Ln^{2+}	n	Exp. $\chi_M T$[a]	$\chi_M T$ $4f^n5d_{z^2}{}^1$ Scenario 1 ($L-S$ coupling)[b]	$\chi_M T$ $4f^n5d_{z^2}{}^1$ Scenario 2 ($J-s$ coupling)	$\chi_M T$ $4f^{n+1}$
La	0	–	0.38	0.38	0.80
Ce	1	1.02	0.33	1.18	1.60
Pr	2	2.05	0.88	1.98	1.64
Nd	3	1.77	0.90	2.01	0.90
Pm	4	–	0.39	1.28	0.09
Sm	5	–	–	0.46	–
Eu	6	7.92	1.50	0.38	7.88
Gd	7	10.00	10.00	8.25	11.81
Tb	8	12.72	14.42	12.19	14.17
Dy	9	15.15	17.01	14.54	14.06
Ho	10	15.17	16.90	14.44	11.48
Er	11	13.20	14.06	11.85	7.15
Tm	12	2.76	9.23	7.52	2.57
Yb	13	–	3.91	2.95	–
Lu	14	–	0.38	0.38	–

[a]All $\chi_M T$ data are reported in units of emu K/mol and were collected at 300 K under an applied field of 10 kOe. [b]Scenario 3 predicts $\chi_M T$ values that are identical to those predicted by Scenario 1.

Here, with the goal of anchoring the evaluation and discussion of spin−orbit coupling in these divalent systems in the context of the greater literature, we note that scenario 1 is formally Russell−Saunders coupling, while scenario 2 can be viewed as an approximation of a $J_{4f}-s$ coupling model. For the latter, the case of spin−spin coupling < k_BT would give rise to ground and first excited multiplets that are not thermally isolated and approach equal population at room temperature. Although trivalent and traditional divalent lanthanide complexes are well described by $L-S$ coupling, $J-s$ coupling has been invoked to describe spin−orbit coupling in the excited states of gas-phase divalent lanthanide ions.[43,44] We note that in the case of k_BT < 4f spin−5d spin coupling <4f spin−orbit coupling (referred to as scenario 3 hereafter), a $J-s$ coupling model predicts a room temperature $\chi_M T$ value that is the same as that derived in the case of $L-S$ coupling, or scenario 1. An illustration of these different models, the relevant term symbols, and expressions for the magnetic moment is given in Figure 8 and Figure S107 for the case of dysprosium(II). For the trigonal compounds [K(2,2,2-cryptand)][$Ln(N(SiMe_3)_2)_3$] and [K(2,2,2-cryptand)][$LnCp'_3$], the room temperature magnetic susceptibilities were previously discussed as being somewhat better described by scenario 1 ($L-S$ coupling), with the exception of [K(2,2,2-cryptand)][Cp'_3Ce].[13,41] However, we note that scenario 3 is equally likely based purely on the reported $\chi_M T$ magnitudes. Thus,

https://doi.org/10.1021/jacs.2c09880
J. Am. Chem. Soc. 2022, 144, 22193−22201

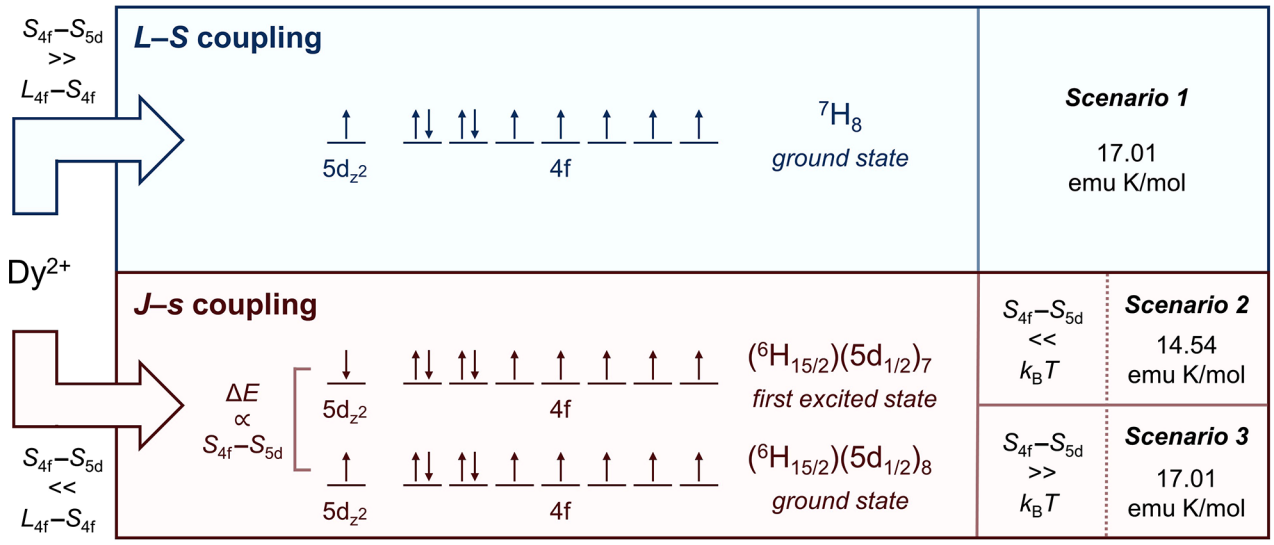

Figure 8. Flowchart illustrating the different spin–orbit coupling scenarios considered in this work for the case of Dy^{2+}; S_{4f}–S_{5d} = spin–spin coupling between 4f and 5d electrons and L_{4f}–S_{4f} = spin–orbit coupling of the 4f shell.

while it is not possible to estimate the relative strengths of the spin–spin and spin–orbit coupling in the trigonal compounds using these models, we can conclude that the spin–spin coupling strength is greater than k_BT (~200 cm^{-1} at 300 K).

The experimental χ_MT values for $Tb(Cp^{iPr5})_2$ and $Dy(Cp^{iPr5})_2$[14] and the new **1-Ln** (Ln = Ce, Pr, Nd, Gd, Ho, Er) complexes at 300 K are given in Table 1, along with the predicted χ_MT values based on scenarios 1/3 and scenario 2. In contrast to $[K(2,2,2\text{-cryptand})][Ln(N(SiMe_3)_2)_3]$ and $[K(2,2,2\text{-cryptand})][LnCp'_3]$, on the whole $Tb(Cp^{iPr5})_2$, $Dy(Cp^{iPr5})_2$, **1-Ce**, **1-Pr**, **1-Nd**, and **1-Ho** exhibit χ_MT values that are more consistent with those predicted from scenario 2, the approximation based on *J*–*s* coupling in the limit of spin–spin coupling < k_BT (Table 1, Figure 7). We surmise that larger 6s character in the HOMO of the linear divalent compounds $Tb(Cp^{iPr5})_2$, $Dy(Cp^{iPr5})_2$, and **1-Ln** relative to the trigonal compounds—supported by our EPR spectroscopy results for **1-Y** and **1-La**—may explain this difference between the two series. Indeed, because of the greater 6s character in the $5d_{z^2}$/6s HOMO of **1-Ln**, spin–spin coupling between the $5d_{z^2}$ and the 4f electrons in those compounds is expected to be weaker than in the previously studied trigonal compounds. Interestingly, for the later Ln = Tb, Dy, Ho, and Er complexes, χ_MT slightly increases toward the values predicted from *L*–*S* coupling, an effect most pronounced for **1-Er**. Finally, **1-Gd** is an outlier among the **1-Ln**, with a room temperature χ_MT value of 10.00 emu K/mol that is consistent with that previously determined for the trigonal Ln^{2+} compounds. Spectroscopic investigations into the nature of the electronic coupling in these linear **1-Ln** complexes are ongoing.

CONCLUSIONS

We have reported the synthesis and characterization of the linear metallocene complexes $Ln(Cp^{iPr5})_2$ (**1-Ln**) for the entire lanthanide series (excluding Pm) and yttrium. These compounds were prepared via salt metathesis of LnI_3 and $NaCp^{iPr5}$ followed by reduction with KC_8 (for Ln = Y, La, Ce, Pr, Nd, Gd, Tb, Dy, and Er); salt metathesis of LnI_3 and $NaCp^{iPr5}$ and in situ reduction with excess $NaCp^{iPr5}$ (Ln = Tm, Lu); or salt metathesis from LnI_2 and $NaCp^{iPr5}$ (Ln = Sm, Eu, Yb). Notably, **1-Y**, **1-La**, **1-Ce**, **1-Pr**, **1-Nd**, **1-Gd**, **1-Ho**, **1-Er**, **1-Tm**, and **1-Lu** constitute the first examples of neutral linear metallocenes for the corresponding elements. Detailed characterization of **1-Ln** using single-crystal X-ray diffraction and UV–vis spectroscopy supports assignment of a $4f^{n+1}$ electron configuration for **1-Sm**, **1-Eu**, **1-Tm**, and **1-Yb** and a $4f^n5d_{z^2}{}^1$ configuration for the remainder of the **1-Ln** series. Interestingly, analysis of **1-Y** and **1-La** using EPR spectroscopy suggests that the linear coordination geometry of **1-Ln** facilitates greater s–d mixing than in the case of $[K(2,2,2\text{-cryptand})][LnCp'_3]$, which also possess a $4f^n5d_{z^2}{}^1$ (or $4d_{z^2}{}^1$) electron configuration. As a result of the high degree of s–d mixing in **1-Y** and **1-La**, these compounds exhibit the largest isotropic hyperfine coupling constants reported to date for molecular compounds of Y^{2+} or La^{2+}. A comparison of the experimental room temperature molar magnetic susceptibilities of **1-Ln** (Ln = Ce, Pr, Nd, Tb, Dy, Ho, and Er) with those reported for trigonal Ln^{2+} compounds suggests that the greater degree of s–d mixing also leads to weaker spin–spin coupling between the 4f and $5d_{z^2}$ electrons. In sum, this study demonstrates the substantial impact of coordination geometry on the electronic structure and magnetic properties of Ln^{2+} compounds. Further investigation into the relationship between coordination geometry and electronic structure in these divalent metallocene complexes is ongoing in our laboratories.

ASSOCIATED CONTENT

Supporting Information

The Supporting Information is available free of charge at https://pubs.acs.org/doi/10.1021/jacs.2c09880.

Synthetic procedures, cyclic voltammetry, IR, NMR, EPR and UV–vis spectroscopy, X-ray crystallography refinement details, and magnetic measurements. (PDF)

AUTHOR INFORMATION

Corresponding Authors

Jeffrey R. Long – *Department of Chemistry and Department of Chemical and Biomolecular Engineering, University of California—Berkeley, Berkeley, California 94720, United States; Materials Sciences Division, Lawrence Berkeley*

https://doi.org/10.1021/jacs.2c09880
J. Am. Chem. Soc. 2022, 144, 22193–22201

National Laboratory, Berkeley, California 94720, United States; orcid.org/0000-0002-5324-1321; Email: jrlong@berkeley.edu

Benjamin G. Harvey − *Research Department, Chemistry Division, US Navy, Naval Air Warfare Center, Weapons Division, China Lake, California 93555, United States;* orcid.org/0000-0003-2091-3539; Email: benjamin.g.harvey.civ@us.navy.mil

Authors

K. Randall McClain − *Research Department, Chemistry Division, US Navy, Naval Air Warfare Center, Weapons Division, China Lake, California 93555, United States*

Colin A. Gould − *Department of Chemistry, University of California—Berkeley, Berkeley, California 94720, United States;* Present Address: Colin A. Gould − Department of Chemistry, Princeton University, Princeton, New Jersey 08544, United States; orcid.org/0000-0001-9539-1582

David A. Marchiori − *Department of Chemistry, University of California—Davis, Davis, California 95616, United States;* Present Address: David A. Marchiori - Department of Chemistry, University of California, Berkeley, Berkeley, California 94720, United States; orcid.org/0000-0001-9738-3674

Hyunchul Kwon − *Department of Chemistry, University of California—Berkeley, Berkeley, California 94720, United States*

Trisha T. Nguyen − *Department of Chemistry, University of California—Davis, Davis, California 95616, United States*

Kyle E. Rosenkoetter − *Research Department, Chemistry Division, US Navy, Naval Air Warfare Center, Weapons Division, China Lake, California 93555, United States;* Present Address: Kyle E. Rosenkoetter - Ernest & Young LLP, EY-Parthenon, Transaction Strategy and Execution Division, Mclean, Virginia 22102, United States

Diana Kuzmina − *Department of Chemistry and Photon Science Institute, University of Manchester, Manchester M13 9PL, U.K.;* orcid.org/0000-0003-3532-5393

Floriana Tuna − *Department of Chemistry and Photon Science Institute, University of Manchester, Manchester M13 9PL, U.K.*

R. David Britt − *Department of Chemistry, University of California—Davis, Davis, California 95616, United States;* orcid.org/0000-0003-0889-8436

Complete contact information is available at: https://pubs.acs.org/10.1021/jacs.2c09880

Author Contributions

○K.R.M. and C.A.G. contributed equally.

Notes

The authors declare no competing financial interest.

■ ACKNOWLEDGMENTS

This work was funded by the Naval Air Warfare Center Weapons Division (NAWCWD) NISE-219 program (K.R.M., B.G.H), NSF grants CHE-1800252 and CHE-2102603 (C.A.G., H.K., J.R.L.), and NIH grant 1R35GM126961-01 (D.A.M., T.T.N., R.D.B.). We thank the NSF for support of C.A.G. through a graduate research fellowship and the National UK EPR Facility at Manchester for support with some of the EPR measurements. We also thank Dr. Katie R. Meihaus for editorial assistance.

■ REFERENCES

(1) Cotton, S. A. *Lanthanide and Actinide Chemistry*; Wiley: New York, 2006; pp 1−7.

(2) Evans, W. J. The Importance of Questioning Scientific Assumptions: Some Lessons from f Element Chemistry. *Inorg. Chem.* **2007**, *46*, 3435−3449.

(3) Bochkarev, M. N.; Fedushkin, I. L.; Fagin, A. A.; Petrovskaya, T. V.; Ziller, J. W.; Broomhall-Dillard, R. N. R.; Evans, W. J. Synthesis and Structure of the First Molecular Thulium(II) Complex: $[TmI_2(MeOCH_2CH_2OMe]_3$. *Angew. Chem., Int. Ed.* **1997**, *36*, 133−135.

(4) Evans, W. J.; Allen, N. T.; Ziller, J. W. The Availability of Dysprosium Diiodide as a Powerful Reducing Agent in Organic Synthesis: Reactivity Studies and Structural Analysis of $DyI_2(DME)_3$ and Its Naphthalene Reduction Product. *J. Am. Chem. Soc.* **2000**, *122*, 11749−11750.

(5) Hitchcock, P. B.; Lappert, M. F.; Maron, L.; Protchenko, A. V. Lanthanum Does Form Stable Molecular Compounds in the + 2 Oxidation State. *Angew. Chem., Int. Ed.* **2008**, *47*, 1488−1491.

(6) MacDonald, M. R.; Ziller, J. W.; Evans, W. J. Synthesis of a Crystalline Molecular Complex of Y^{2+}, $[(18\text{-crown-}6)K][(C_5H_4SiMe_3)_3Y]$. *J. Am. Chem. Soc.* **2011**, *133*, 15914−15917.

(7) MacDonald, M. R.; Bates, J. E.; Fieser, M. E.; Ziller, J. W.; Furche, F.; Evans, W. J. Expanding Rare-Earth Oxidation State Chemistry to Molecular Complexes of Holmium(II) and Erbium(II). *J. Am. Chem. Soc.* **2012**, *134*, 8420−8423.

(8) MacDonald, M. R.; Bates, J. E.; Ziller, J. W.; Furche, F.; Evans, W. J. Completing the Series of + 2 Ions for the Lanthanide Elements: Synthesis of Molecular Complexes of Pr^{2+}. Gd^{2+}, Tb^{2+}, and Lu^{2+}. *J. Am. Chem. Soc.* **2013**, *135*, 9857−9868.

(9) Fieser, M. E.; MacDonald, M. R.; Krull, B. T.; Bates, J. E.; Ziller, J. W.; Furche, F.; Evans, W. J. Structural, Spectroscopic, and Theoretical Comparison of Traditional vs Recently Discovered Ln^{2+} Ions in the $[K(2.2.2\text{-cryptand})][(C_5H_4SiMe_3)_3Ln]$ Complexes: The Variable Nature of Dy^{2+} and Nd^{2+}. *J. Am. Chem. Soc.* **2015**, *137*, 369−382.

(10) Evans, W. J.; Allen, N. T.; Ziller, J. W. ″Expanding divalent organolanthanide chemistry: the first orgaothulium(II) complex and the in situ organodysprosium(II) reduction of dinitrogen.″. *Angew. Chem., Int. Ed.* **2002**, *41*, 359−361.

(11) Ariciu, A.-M.; Woen, D. H.; Huh, D. N.; Nodaraki, L. E.; Kostopoulos, A. K.; Goodwin, C. A. P.; Chilton, N. F.; McInnes, E. J. L.; Winpenny, R. E. P.; Evans, W. J.; Tuna, F. Engineering electronic structure to prolong relaxation times in molecular qubits by minimizing orbital angular momentum. *Nat. Commmun.* **2019**, *10*, 3330.

(12) Gould, C. A.; McClain, K. R.; Reta, D.; Kragskow, J. G. C.; Marchiori, D. A.; Lachman, E.; Choi, E.-S.; Analytis, J. G.; Britt, R. D.; Chilton, N. F.; Harvey, B. G.; Long, J. R. Ultrahard magnetism from mixed-valence dilanthanide complexes with metal-metal bonding. *Science* **2022**, *375*, 198−202.

(13) Meihaus, K. R.; Fieser, M. E.; Corbey, J. R.; Evans, W. J.; Long, J. R. Record High Single-Ion Magnetic Moments through $4f^n5d^1$ Electron Configurations in the Divalent Lanthanide Complexes $[(C_5H_4SiMe_3)_3Ln]^-$. *J. Am. Chem. Soc.* **2015**, *137*, 9855−9860.

(14) Gould, C. A.; McClain, K. R.; Yu, J. M.; Groshens, T. J.; Furche, F.; Harvey, B. G.; Long, J. R. Synthesis and Magnetism of Neutral, Linear Metallocene Complexes of Terbium(II) and Dysprosium(II). *J. Am. Chem. Soc.* **2019**, *141*, 12967−12973.

(15) Jaroschik, F.; Nief, F.; Ricard, L. Synthesis of a new stable, neutral organothulium(II) complex by reduction of a thulium(III) precursor. *Chem. Commun.* **2006**, *4*, 426−428.

(16) Jaroschik, F.; Nief, F.; Le Goff, X.-F.; Ricard, L. Isolation of Stable Organodysprosium(II) Complexes by Chemical Reduction of Dysprosium(III) Precursors. *Organometallics* **2007**, *26*, 1123−1125.

(17) Sitzmann, H.; Dezember, T.; Schmitt, O.; Weber, F.; Wolmershäuser, G.; Ruck, M. Metallocenes of Samarium, Europium, and Ytterbium with the Especially Bulky Cyclopentadienyl Ligands

$C_5H(CHMe_2)_4$, $C_5H_2(CMe_3)_3$, and $C_5(CHMe_2)_5$. *Z. Anorg. Allg. Chem.* **2000**, *626*, 2241−2244.
(18) Evans, W. J.; Hughes, L. A.; Hanusa, T. P. Synthesis and crystallographic characterization of an unsolvated, monomeric samarium bis(pentamethylcyclopentadienyl) organolanthanide complex, $(C_5Me_5)_2Sm$. *J. Am. Chem. Soc.* **1984**, *106*, 4270−4272.
(19) Kaupp, M.; Schleyer, P. v. R.; Dolg, M.; Stoll, H. The Equilibrium Structures of Monomeric Group 2 and Lanthanide(II) Metallocenes MCp_2 (M = Ca, Sr, Ba, Sm, Eu, Yb) Studied by ab Initio Calculations. *J. Am. Chem. Soc.* **1992**, *114*, 8202−8208.
(20) Visseaux, M.; Barbier-Baudry, D.; Blacque, O.; Hafid, A.; Richard, P.; Weber, F. New base-free metallocenes of samarium and neodymium, an approach to stereoelectronic control in organolanthanide chemistry. *New J. Chem.* **2000**, *24*, 939−942.
(21) Weber, F.; Sitzmann, H.; Schultz, M.; Sofield, C. D.; Andersen, R. A. Synthesis and Solid State Structures of Sterically Crowded d^0-Metallocenes of Magnesium, Calcium, Strontium, Barium, Samarium, and Ytterbium. *Organometallics* **2002**, *21*, 3139−3146.
(22) Evans, W. J.; Perotti, J. M.; Brady, J. C.; Ziller, J. W. Tethered Olefin Studies of Alkene versus Tetraphenylborate Coordination and Lanthanide Olefin Interactions in Metallocenes. *J. Am. Chem. Soc.* **2003**, *125*, 5204−5212.
(23) Nocton, G.; Ricard, L. N-aromatic heterocycle adducts of bulky $[1,2,4\text{-}(Me_3C)_3C_5H_2]_2Sm$: synthesis, structure and solution analysis. *Dalton Trans.* **2014**, *43*, 4380−4387.
(24) Kilpatrick, A. F. R.; Cloke, F. G. N. A base-free synthetic route to anti-bimetallic lanthanide pentalene complexes. *Dalton Trans.* **2017**, *46*, 5587−5597.
(25) Palumbo, C. T.; Ziller, J. W.; Evans, W. J. Structural characterization of the bent metallocenes, $[C_5H_3(SiMe_3)_2]_2Sm$ and $[C_5H_3(CMe_3)_2]_2Ln$ (Ln = Eu, Sm), and the mono(cyclopentadienyl) tetraphenylborate complex, $[C_5H_3(CMe_3)_2]Eu(\mu\text{-}\eta^6\text{:}\ \eta^1\text{-}Ph)_2BPh_2$. *J. Organomet. Chem.* **2018**, *867*, 142−148.
(26) Ruspic, C.; Moss, J. R.; Schürmann, M.; Harder, S. Remarkable Stability of Metallocenes with Superbulky Ligands: Spontaneous Reduction of Sm^{III} to Sm^{II}. *Angew. Chem., Int. Ed.* **2008**, *47*, 2121−2126.
(27) van Velzen, N. J. C.; Harder, S. Deca-Arylsamarocene: An Unusually Inert Sm(II) Sandwich Complex. *Oranometallics* **2018**, *37*, 2263−2271.
(28) Anderson, L. B.; Macero, D. J. The Formal Reduction Potential of the Europium(III)-Europium(II) System. *J. Phys. Chem.* **1963**, *67*, 1942.
(29) Mikheev, N. B.; Aurman, L. N.; Rumer, I. A. Correlation between Oxidation Potentials of the Lanthanides in Aqueous Solutions and Chloride Melts. *Inorg. Chim. Acta* **1985**, *109*, 217−220.
(30) Szostak, M.; Spain, M.; Procter, D. J. Uncovering the Importance of Proton Donors in TmI_2-Promoted Electron Transfer: Facile C-N Bond Cleavage in Unactivated Amides. *Angew. Chem., Int. Ed.* **2013**, *52*, 7237−7241.
(31) Sitzmann, H.; Bock, H.; Boese, R.; Dezember, T.; Havlas, Z.; Kaim, W.; Moscherosch, M.; Zanathy, L. Pentaisopropylcyclopentadienyl: Singlet Anion, Doublet Radical, Triplet Cation of a Carbocyclic π System. *J. Am. Chem. Soc.* **1993**, *115*, 12003−12009.
(32) Harder, S.; Naglav, D.; Ruspic, C.; Wickleder, C.; Adlung, M.; Hermes, W.; Eul, M.; Pöttgen, R.; Rego, D. B.; Poineau, F.; Czerwinski, K. R.; Herber, R. H.; Nowik, I. Physical Properties of Superbulky Lanthanide Metallocenes: Synthesis and Extraordinary Luminescence of $[Eu^{II}(Cp^{BIG})_2]$ (Cp^{BIG} = $(4\text{-}n\text{Bu-}C_6H_4)_5$-Cyclopentadienyl. *Chem.—Eur. J.* **2013**, *19*, 12272−12280.
(33) Morton, J. R.; Preston, K. F. Atomic parameters for paramagnetic resonance data. *J. Magn. Reson.* **1978**, *30*, 577−582.
(34) Cassani, C. M.; Duncalf, D. J.; Lappert, M. F. The First Example of a Crystalline Subvalent Organolanthanum Complex: $[K([18]crown\text{-}6)\text{-}(\eta^2\text{-}C_6H_6)_2][(LaCp^{tt}_2)_2(\mu\text{-}\eta^6\text{:}\eta^6\text{-}C_6H_6)]\bullet 2C_6H_6$ ($Cp^{tt} = \eta^5\text{-}C_5H_3But_2\text{-}1,3$). *J. Am. Chem. Soc.* **1998**, *120*, 12958−12959.
(35) Kundu, K.; White, J. R. K.; Moehring, S. A.; Yu, J. M.; Ziller, J. W.; Furche, F.; Evans, W. J.; Hill, S. A 9.2 GHz clock transition in a Lu(II) molecular spin qubit arising from a 3,467-MHz hyperfine interaction. *Nat. Chem.* **2022**, *14*, 392−397.
(36) Jiang, Y.; Li, Z.; Zhang, J.; Wang, Z. Endohedral Metallofullerene $M_2@C_{80}$: A New Class of Magnetic Superhalogen. *J. Phys. Chem. C* **2020**, *124*, 2131−2136.
(37) Fang, M.; Lee, D. S.; Ziller, J. W.; Doedens, R. J.; Bates, J. E.; Furche, F.; Evans, W. J. Synthesis of the $(N_2)^{3-}$ Radical from Y^{2+} and Its Protonolysis Reactivity To Form $(N_2H_2)^{2-}$ via the $Y[N(SiMe_3)_2]_3/KC_8$ Reduction System. *J. Am. Chem. Soc.* **2011**, *133*, 3784−3787.
(38) Moehring, S. A.; Miehlich, M.; Hoerger, C. J.; Meyer, K.; Ziller, J. W.; Evans, W. J. A Room-Temperature Stable Y(II) Aryloxide: Using Steric Saturation to Kinetically Stabilize Y(II) Complexes. *Inorg. Chem.* **2020**, *59*, 3207−3214.
(39) Bao, L.; Chen, M.; Pan, C.; Yamaguchi, T.; Kato, T.; Olmstead, M. M.; Balch, A. L.; Akasaka, T.; Lu, X. Crystallographic Evidence for Direct Metal-Metal Bonding in a Stable Open-Shell $La_2@I_h\text{-}C_{80}$ Derivative. *Ang. Chem. Int. Ed.* **2016**, *55*, 4242−4246.
(40) In our previous report on the synthesis and magnetism of $Dy(Cp^{iPr5})_2$ and $Tb(Cp^{iPr5})_2$,[14] we describe scenario 2 as "*j*−*j* coupling." Here, we instead use the more precise nomenclature *J*−*s* coupling to emphasize that the spin of the 5d electron (*s*) couples to the total angular momentum of the 4f shell (*J*) in this spin−orbit coupling scheme.
(41) Ryan, A. J.; Darago, L. E.; Balasubramani, S. G.; Chen, G. P.; Ziller, J. W.; Furche, F.; Long, J. R.; Evans, W. J. Synthesis, Structure, and Magnetism of Tris(amide) $[Ln\{N(SiMe_3)_2\}_3]^{1-}$ Complexes of the Non-traditional + 2 Lanthanide Ions. *Chem.—Eur. J.* **2018**, *24*, 7702−7709.
(42) Anderson, D. M.; Cloke, F. G. N.; Cox, P. A.; Edelstein, N.; Green, J. C.; Pang, T.; Sameh, A. A.; Shalimoff, G. On the Stability and Bonding in Bis(η-arene)lanthanide Complexes. *J. Chem. Soc., Chem. Commun.* **1989**, 53−55.
(43) Wybourne, B. G. *Spectroscopic Properties of the Rare Earths*; Interscience: New York, 1965; pp 49−63.
(44) Bryant, B. W. Spectra of Doubly and Triply Ionized Ytterbium, Yb III and Yb IV. *J. Opt. Soc. Am.* **1965**, *55*, 771−779.

https://doi.org/10.1021/jacs.2c09880
J. Am. Chem. Soc. 2022, 144, 22193−22201